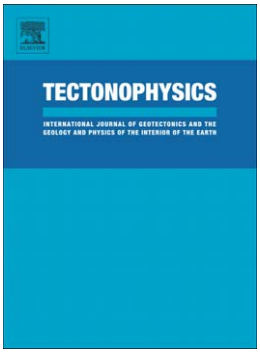

The influence of mechanical stiffness on caldera deformation and implications for the 1971-1984 Rabaul uplift (Papua New Guinea)

A. Geyer, J. Gottsmann

PII: S0040-1951(09)00626-X
DOI: doi: 10.1016/j.tecto.2009.10.029
Reference: TECTO 124791

To appear in: *Tectonophysics*

Received date: 27 April 2009
Revised date: 30 October 2009
Accepted date: 30 October 2009

Please cite this article as: Geyer, A., Gottsmann, J., The influence of mechanical stiffness on caldera deformation and implications for the 1971-1984 Rabaul uplift (Papua New Guinea), *Tectonophysics* (2009), doi: 10.1016/j.tecto.2009.10.029

The influence of mechanical stiffness on caldera deformation and implications for the 1971-1984 Rabaul uplift (Papua New Guinea)

Geyer, A.[1,2] and Gottsmann, J.[1]

1 Department of Earth Sciences, University of Bristol, UK , Wills Memorial Building, Queen's Road BS8 1RJ, Bristol, UK

2 Now at: CIMNE International Center for Numerical Models in Engineering, UPC Campus Norte , Edificio C1, C/ Gran Capitán s/n , 08034 Barcelona, Spain

Corresponding author: ageyer@cimne.upc.edu

Keywords: ground deformation, numerical modelling, caldera, mechanical stiffness, volcano

Abstract: Numerical models provide a link between measured ground deformation and the inaccessible deformation source, and here we present a systematic set of new results from numerical forward modelling using a Finite Element Method with application to volcano geodesy. We first provide a generic case analysis and then evaluate ground deformation data from the Rabaul caldera in Papua New Guinea. The generic case simulates surface displacements in a flat-topped caldera setting due to pressure changes in a shallow (at 5 km depth) oblate reservoir overlain by host rock with variable mechanical stiffness. Our main findings are: i) the amplitude and wavelength of resultant ground deformation is dependent on the distribution of mechanically stiff and soft lithologies and their relative distribution above the reservoir, ii) for a given pressure change, surface displacement may be amplified by the presence of soft layers compared to generic simulations using a homogenous background medium, and iii) the ratio of maximum horizontal over maximum vertical deformation ($u_{xx}max/u_{yy}max$) is particularly sensitive to the presence of rock heterogeneities.

In assessing the influence of mechanical heterogeneities (as derived form seismic data) in caldera-fill successions on ground deformation at Rabaul we apply our model to inform on the source causing uplift between 1971 and 1984. The best-fit model involves a combination of two oblate sources at 3 and 1 km depth, respectively, beneath the centre of the caldera undergoing a reasonable pressure increment (~38 MPa), compared to unrealistic pressurization if modelled using a homogeneous background medium.

1. Introduction

One of the most common signals of volcanic unrest is ground deformation. Various source mechanisms have been proposed to explain observed volcano deformation including magma intrusion, slip along faults, or pore pressure variations in transient hydrothermal systems (Dzurisin and Johnston, 2003; Poland et al., 2006a; Masterlark, 2007). Some sources may be cause for concern, e.g. pressure changes in shallow magma reservoirs or intrusive events, while others may not. Herein lays a fundamental problem for volcano geodesy since it is difficult to directly identify causative processes at depth. As a consequence deformation sources need to be inferred by the analysis of observables. Models provide one link between measured ground deformation and the inaccessible deformation source. Substantial effort has therefore gone into the development of inverse and forward prediction schemes that strive to characterize source properties from recorded ground deformation data and vice versa.

One resource to inform on causative processes of volcano deformation is the finite element method (FEM). In their pioneering work, Dieterich and Decker (1975) investigated resultant ground deformation at the surface induced by pressure sources embedded in a homogeneous, isotropic, Poisson-solid half-space. Subsequent FEM-based studies investigated, for example, sensitivities to the geometry of the expanding source (Yang et al., 1988) and time-dependent effects (Newman et al., 2001, 2006) in a homogeneous, isotropic, Poisson-solid half-space. Others used FEMs to explore stress distribution and ground deformation accounting for heterogeneous caldera configurations, structural discontinuities or topography (De Natale and Pingue, 1993, 1996; De Natale et al., 1997; Williams and Wadge, 1998; Orsi et al., 1999; Trasatti et

al., 2003, 2005; Troise et al., 2003; Bonaccorso et al., 2005; Folch and Gottsmann, 2006; Poland et al., 2006b).

Expanding on existing work (e.g. Bianchi et al., 1987) , we present results from numerical considerations of volcano deformation within the mathematical concept of heterogeneous elastic media.

In the first part of this paper, we present a set of new results from numerical forward modelling. We simulate the theoretically resultant vertical and horizontal deformation in a volcanic area as the response of an elastic medium to pressure changes in a reservoir surrounded by host rock with variable mechanical properties. Although the evaluation of purely elastic behaviour to predict brittle rock strain is perhaps not as robust as a full description of all mechanical behaviour, it is a good enough approximation for the purpose of this study. We show that medium heterogeneities such as layering of mechanically stiff and soft rocks may induce significant variations in the stress field that contribute to modify the ground deformation pattern at the free surface. The focus here is on a flat-topped collapse caldera system, where we find that varying mechanical properties of caldera-fill successions results in a significant distortion of the predicted deformation pattern if compared with model results based on the assumption of mechanical homogeneity. Application of the model in the second part of the paper informs on the causative source of ground inflation between 1971 and 1984 at Rabaul caldera (Papua New Guinea).

2. Procedure

2.1 Background

In the present work, we assume that during ground deformation due to reservoir expansion, the surrounding crust behaves as an homogeneous linear elastic material. For the purpose of this paper it is irrelevant whether the reservoir be of magmatic (molten rock, crystals and volatiles) or hydrothermal (aqueous fluid phase and gas) nature or a hybrid of both. We are concerned here with the resultant ground deformation patterns rather than the nature of the causative processes leading to ground deformation, be it: injection of new magma, a critical stage of magma differentiation, or some other perturbation.

For each model the theoretical displacement and stress field has have been obtained using FEMFES, a code that solves elasticity by means of a Finite Element Method with nodal implementation (Codina and Folch, 2004).

2.2 Geometrical setting and boundary conditions

The models involve an axially-symmetric computational domain, which corresponds to an idealized cross-section of the upper crust of 50 km length and 25 km depth below a flat surface (Fig. 1a). The reservoir is modelled as an ellipsoidal cavity of length a (width $2a$) and b (height $2b$). In all generic models we set a=2.5 km and b=0.75 km (Fig. 1a). The upper planar surface of each scenario corresponds to the Earth's surface and is treated as a free surface (i.e. traction free). The inflating reservoir is represented by a uniformly distributed overpressure ΔP of 15MPa around the magma chamber walls (Fig.1a). Displacements are prescribed to zero on the computational margins, placed at vertical and radial distances several times greater than the dimensions of the reservoir, i.e. where the variations of the stress field due to the reservoir can be neglected. More precisely, our results are mainly focused on the central

and shallowest part of the computational domain (Fig.1a). The computational area is large enough (50 × 25 km) in order to avoid possible wall effects.

FIGURE 1

2.3 Variations considered in the different runs

Mechanical heterogeneity is simulated by different layers with either high (stiff material) or low (soft materials) Young's moduli (E) (Table 1). We define for depths between 1000 and 4500 m, up to seven different layers of 500 m thickness each (Fig. 1b). Soft layers are represented by E = 18 GPa, ρ = 2200 kg/m^3 while stiff layers have E = 72 GPa and ρ = 2800 kg/m^3 (Fig. 1b). If two consecutive layers A and B with thicknesses T_A and T_B , respectively, have the same mechanical properties, they are considered as a single layer of thickness $T_A + T_B$. In the model simulating a homogeneous medium, all seven layers and the remaining host rock have the same mechanical properties: E = 45 GPa and ρ = 2500 kg/m^3. Poisson's coefficient (ν) is kept constant ($\nu = 0.25$), as it has been shown to have very little influence on results presented in this work (e.g. Gudmundsson , 2007).

We note here that the range of selected Young's moduli in the models is quite modest (from 18 to 72 GPa) compared to published data, which indicate values from below 1 GPa to more than 100 GPa (e.g. Gudmundsson and Brenner, 2004; Gudmundsson, 2006) in volcanic successions, representing a variability over more than 2 order of magnitude in the most extreme cases. It is hence important to point out, that the aim of the generic model is to demonstrate that even for modest variations in E,

ground deformation patterns are significantly different compared to results from models solving for mechanical homogeneity. Effects are amplified with increased contrasts in the mechanical stiffness of encasing rocks. Equally, in the opposite sense, the smaller the contrast in stiffness, the more similar the results to those from models assuming mechanical homogeneity.

The first set of numerical runs (Fig. 2a, Table 2) are performed accounting for either one stiff *or* one soft layer with variable layer thickness (**T)**. In the subsequent runs we simulate two different layers, one soft and one stiff, with thicknesses T_{SL} and T_{HL}, respectively. We explore the effect on ground deformation when varying the ratio between the thicknesses of both layers (**RLT**) (Fig. 2b, Table 2) and the distance between both layers (**DL**) (Fig. 2c, Table 2). Additionally, we are interested in exploring the influence of the distribution pattern (**LDP**) between stiff or soft layers on the ground displacement (Fig. 2d, Table 2).

TABLE 1

FIGURE 2

TABLE 2

3. Results and discussion of generic models

3.1 Comparison to homogenous media

For each run, we analyze the vertical and horizontal displacement at the free surface, u_{yy} and u_{xx}, respectively. For those cases exploring the influence of host rock heterogeneity, we compare and plot the results with the reference homogeneous model (u_{yyHOMO} and u_{xxHOMO}) and also normalize u_{yy} and u_{xx} to u_{yyHOMO} and u_{xxHOMO}.

In general terms, compared to the homogeneous result, the presence of mechanically different layers does neither modify the shape nor the wavelength or footprint (i.e. the total zone affected by deformation) of the overall ground deformation. What changes when varying mechanical properties is the amplitude of either deformation depending on the thickness of the soft/stiff layers. Compared to the results obtained by the homogenous run, for the same reservoir pressurization, thick soft layers lead to a measurable increase in the amplitude, i.e. an increase in both the u_{yy}max and u_{xx}max values (Figs. 3a and 3e). Regarding the u_{yy} curve, results indicate that amplitude differences with respect to the homogenous results become significant once more than a 30% of the material located above the upper surface of the reservoir is made up by soft material. Contrarily, the presence of thick stiff layers reduces the amplitude, i.e. decreases u_{yy}max (Figs. 3b and 3f). Regarding horizontal displacements, results obtained indicate that if overlying material is composed of soft layers u_{xx}max increases (Fig. 3c and 3g), whereas the same parcel of stiff layers would decrease u_{xx}max (Fig. 3d and 3h), compared to homogeneous results.

FIGURE 3

3.2 Alternating lithologies

In the presence of both soft and stiff layers, results obtained are considerably different. For example, if the soft layer is located at shallower depth and T_{SL} :T_{HL} = 3:4 (T_{SL} :T_{HL} = 3×500 m : 4×500 m= 1500 m :2000 m) the possible effect of either layers on u_{yy} cancels out (Fig. 4a and 4e) and there is no marked difference to the homogenous result. However, for higher ratios of T_{SL}:T_{HL} (T_{SL}:T_{HL} = 5:2 ; 7:0) the amplification

induced by the soft shallow layers (u_{yy}max > u_{yy}max$_{HOMO}$) exceeds the attenuation caused by the stiff layers (u_{yy}max < u_{yy}max$_{HOMO}$) and the results indicate a reasonable increase of u_{yy}max. Contrarily, for T_{SL} :T_{HL} = 2 : 5, the effect of the stiff layer is more marked than that of the soft layers and thus u_{yy}max tends to fall below the homogeneous result. In case stiff layers overlie soft layers, a 500 m thick soft layer may cancel out the effect caused by a 3500 m thick pile of stiff layers, i.e. the closer the soft layer to the reservoir, the higher its amplification of ground deformation (Figs. 4b and 4f).

FIGURE 4

In more detail, comparing the results obtained for the runs MS-4S (T_{SL} = 4×500 m = 2000 m) (Fig. 3a) with those from run MS-4:3S (T_{SL} :T_{HL} = 4×500 m : 3·500 m= 2000 m : 1500 m) (Fig. 4a), run MS-4S gives u_{yy}max = 1.68 m, whereas run MS-4:3S gives 1.53 m. Although the soft layers of run MS-4:3S amplify u_{yy}max in comparison to the homogeneous result, underlying stiff layers dim this effect by reducing u_{yy}max by about 10%. By contrast, run MS-4H (T_{HL} = 4×500 m = 2000 m) (Fig. 3b) compared to MS-4:3H (T_{HL} :T_{SL} = 4×500 m : 3×500 m= 2000 m : 1500 m) (Fig. 4b), we obtain u_{yy}max = 1.35 m, compared to 1.73 m, respectively. Thus, although stiff layers tend to reduce u_{yy}max compared to the homogeneous result, the underlying soft layers overcomes this effect by amplifying u_{yy}max to the extent that u_{yy}max > u_{yy}max$_{HOMO}$.

Similar to the distribution of u_{yy} at surface, soft layers located at shallower levels and several times thicker than stiff layers, considerably increase the amplitude of the horizontal deformation. In contrast, shallow stiff layers with an overall thickness exceeding that of deeper soft layers tend to reduce the horizontal deformation at the surface. Comparing results from models MS-4S, MS-4H, MS-4:3H and model MS-4:3S shows that stiff layers located below soft layers tend to reduce u_{xx}max, while soft layers

located below thick stiff layer tend to increase the horizontal displacement at surface. For the case of soft layers overlying stiff layers, the effect of host rock layering is practically cancelled out as soon as the ratio T_{SL} over T_{HL} is between 4:3 (MS-4:3S) and 5:2 (MS-5:2S). By contrast, if stiff material overlies soft material results indicate that the relationship T_{HL} to T_{SL} should be around 5:2 (MS-5:2H) for the respective effects to cancel out.

Concerning the influence of distance between soft and stiff layers, **DL**, on the deformation pattern, if soft layers overlie stiff layers, the amplitudes of both u_{yy} and u_{xx} are independent of **DL** (Fig. 5a and 5c). By contrast, if stiff layers overlie soft layers, increasing the distance between both layers tends to increase u_{yy}max and u_{xx}max compared to the homogeneous model (Fig. 5b and 5d). Again here, we can see that the closer the soft layer to the reservoir, the higher its amplification effect on ground deformation.

FIGURE 5

Independent of their vertical distribution at depth, yet, proportional to their cumulative thickness, stacking of soft layers increases the amplitude of both u_{yy} and u_{xx} compared to the homogeneous result (Fig. 6a and 6b). Accordingly, regardless of their distribution, stiff layers tend to decrease the amplitude of both vertical and horizontal displacements proportionally to their cumulative thickness.

FIGURE 6

3.3 The ratio $u_{xx}max / u_{yy}max$

In agreement with earlier studies (e.g., Dieterich and Decker, 1975), we find that horizontal displacements are far more revealing concerning source properties than are vertical displacements only. We therefore discuss our results by expressing our findings as the dimensionless ratio of u_{xx}max over u_{yy}max. In doing so, results become directly comparable to other (theoretical) studies, which may have employed different values of elastic properties. The ratio of u_{xx}max / u_{yy}max has been used as a sensitivity criterion using homogenous elastic models as to reservoir geometry and depth, whereby values of around 0.3 were found to be common for oblate sources, values of ca. 0.4 for spherical sources, and values > 0.5 are common for prolate spheroids (see below and also Fialko et al., 2001; Troise et al., 2008). We can thus evaluate if these proposed generic relationships still hold true for heterogeneous media.

Figure 7 illustrates the u_{xx}max / u_{yy}max values for the different runs presented in the earlier sections. Each graph also shows the value corresponding to the homogeneous model ($u_{xx}max_{HOMO}$ / $u_{yy}max_{HOMO}$). Results indicate that an increase in T_{SL} (thickness of the soft layer) tends to reduce u_{xx}max / u_{yy}max and, independently of T_{SL} , the ratio's values are consistently lower than values for the homogeneous case (Fig. 7a). Consequently, we infer that soft layers generally modify the amplitude of u_{yy} more profoundly than of u_{xx}. By contrast, the thicker the stiff layer (increase of T_{HL}) the higher u_{xx}max / u_{yy}max, but the slope of this dependency is fairly gentle, i.e. stiff layers equally modify the amplitudes of both u_{xx} and of u_{yy}. However, the values are always close to the homogeneous case ratio. In fact, there is no significant (realistically resolvable) difference compared to the homogeneous result, unless a good 50% or so of the media overlying the reservoir is composed of stiff rock with an about 66% higher Young's modulus compared to background values.

FIGURE 7

Varying the proportion between soft and stiff layers, it is evident that with increasing thickness of the shallow soft layer the ratios u_{xx}max / u_{yy}max tend to decrease, while they increase with increasing thickness of the shallow stiff layer (Fig. 7b). Comparing the results obtained for model MS-5H (Fig. 7a) with those of run MS-5:2H (Fig. 7b), we see that the presence of a 1000 m thick soft layer underlying a 2500 m thick stiff layer tends to considerably reduce u_{xx}max / u_{yy}max . By contrast, the results obtained for run MS-5S (Fig. 7a) and run MS-5:2S (Fig. 7b), show that 1000 m worth of stiff material below 2500 m of soft material only slightly increases u_{xx}max / u_{yy}max .

In summary, based on our axial symmetric analysis, we find that heterogeneities in the mechanical properties of the host rock alter the ratio u_{xx}max / u_{yy}max, by either increasing or decreasing its value, compared to the ratio obtained for a homogenous medium. However, soft layers have a significantly larger effect on altering the ratio compared to stiff layers. The key point here is that assuming that a certain value of u_{xx}max / u_{yy}max is indicative for a specific reservoir (pressure source) geometry or size/depth relationship may be to bold a statement and can lead to erroneous interpretations of source parameters. Deviation from a specific ratio may not necessarily indicate an “incorrect” reservoir geometry. As shown by our results, misfits to observables and deviations from accepted ratios may in fact be controlled by mechanical heterogeneity.

4. Model application to Rabaul caldera (Papua New Guinea)

In the following, we apply our model to inform on the causative process of ground deformation at Rabaul caldera between November 1971 and May 1984.

Rabaul caldera (Papua New Guinea) is a flat-topped collapse caldera system, where mechanical properties of caldera-fill successions are pronouncedly different to surrounding rocks and therefore one might expect significant distortion of resulting ground deformation patterns due to pressure changes in a subsurface reservoir given the results of our generic analysis above.

4.1 Geological setting and ground deformation data

Rabaul caldera itself is the most recently active of four adjoining calderas/volcanic centres along a roughly N-S-trending alignment through the eastern Gazelle Peninsula (Fig. 8a). The caldera has an elliptic (4 × 10 km) shape and was formed by two vertical collapse episodes (about 3.5 and 1.4 ka) accompanying eruption of dacitic ignimbrites, which might have largely filled the collapse depression (Heming and Carmichael, 1973; Heming, 1974, 1977, Nairn et al., 1995) (Fig. 8b). Volcanism at Rabaul caldera has been dominated by two main eruption types: (1) basaltic and andesitic composite cone-building eruptions producing local lava and scoria-fall deposits from vents mostly located on the North-eastern side of the caldera; and (2) dacitic and (rarely) rhyolitic explosive eruptions from vents within or south of the present caldera, producing wide spread ignimbrite and plinian fall deposits, with proximal pyroclastic surges (Wood et al., 1995). The largest of these eruptions were accompanied by caldera collapse. Starting with anomalous seismicity in 1971 the caldera underwent uplift, which peaked in 1984 as part of a dramatic increase in seismic

activity and tumescence (McKee et al. 1984). An eruption did however not occur until 1994.

FIGURE 8

For the purpose of this paper we analyse ground deformation data obtained by annual levelling surveys between November 1971 and May 1984 as reported in Figure 8c of McKee et al. (1984).

4.2 The Rabaul numerical model: Geometry, dimensions, mechanical properties and boundary conditions

We create an axi-symmetrical FEM of Rabaul caldera and surroundings consisting of an idealized cross-section of the upper crust. The model domain is 25 km in length and extending a depth of 25 km below a flat surface (Fig. 9) to circumvent wall effects during computation. In reproducing reservoir location, geometry and subsurface lithology, we employ results from a recent seismic tomographic study (Finlayson et al. 2003).

Figure 8b shows a model of subsurface layering beneath Rabaul as inferred from P-wave velocities (V_p) reported in Finlayson et al. (2003). To obtain mechanical parameters for these obvious variations in lithology with depth, we use a polynomial approximation reported in Brocher (2005) to deduce rock density:

$$\rho = 1.6612\ V_p - 0.4721 V_p^2 - 0.067 V_p^3 - 0.0043\ V_p^4 - 0.000106\ V_p^5 \qquad (1)$$

The equation is calibrated for V_p values between 1.5 and 8.5 km/s and thus appropriate for constraining the shallow subsurface density structure at Rabaul.

In a next step, Young's moduli are obtained for the individual layers via:

$$V_p = \sqrt{\frac{M}{\rho}} \tag{2}$$

where M is the P-wave modulus defined also as:

$$M = E\frac{1-\upsilon}{(1+\upsilon)(1-2\upsilon)} \tag{3}$$

where v is the Poisson ratio which we set to a constant value of 0.25 for our model. The so derived values of ρ and E for the different layers of the model are reported in Figure 9.The thickness of the different layers has been extrapolated from the cross section of V_p values by Finlayson et al. (2003)(Fig. 8b) considering a central log.

The reservoir is modelled as an ellipsoidal cavity of length a = 2 km (width 2a = 4 km) and b = 125 m (height 2b = 250 m), with its upper surface located at a depth of 3000 m. The upper planar surface of each scenario corresponds to the Earth's surface and is treated as a free surface (i.e. traction free). The inflating reservoir is represented by a uniformly distributed overpressure of 30MPa along the reservoir walls (Fig. 9). We derive the geometry of the source from anomalous V_p data reported in Finlayson et al. (2003), which indicate a 2 km thick low velocity zone at 3 km depth. Displacements are prescribed to zero on the computational margins, placed at vertical and radial distances times greater than the dimensions of the reservoir, i.e. where the variations of the stress field due to reservoir pressurization can be neglected as, in fact, we focus our analysis on the central and shallowest part of the computational domain.

FIGURE 9

The mechanically variable subsurface lithologies are modelled considering materials of high (stiff material) or low (soft materials) Young's modulus (E) as shown in Figure 9.

For the purpose of direct comparison, we have also run a matching model in terms of reservoir shape, depth and excess pressure, but considering an isotropic homogeneous media of E=35GPa , ρ = 2300 kg/m^3 and ν = 0.25 . Note, that these values are approximately mean values of the above calculated mechanical properties. We refer to these two models as 1SHT (one source heterogeneous) and 1SHO (one source homogeneous), respectively in the following.

4.3 Results from model simulations

It is evident from the results obtained, that the model accounting for the "realistic?" shallow subsurface lithologies (heterogeneous) performs much better than the model accounting for an isotropic homogeneous medium (Fig. 10). A chi-square (χ^2)-test to compare modelled (M) with observed (O) data (χ^2= Σ[(O-M)^2/M]) gives a value of 0.12 for 1SHT and a value of 0.42 for 1SHO. Despite the simplistic approach in our model we achieve an acceptable fit to the reported data given a reasonable value for reservoir pressurization (within upper limit of tensile strength of surrounding rocks). To fit the amplitude of the ground deformation using a mechanically isotropic homogeneous media of E=35GPa , ρ = 2300 kg/m^3 and ν = 0.25, overpressurisation of around 45 MPa is required; for a slightly stiffer homogeneous media (E=45GPa , ρ =

2300 kg/m^3 and ν = 0.25), a reservoir overpressure of 55MPa is required, both of which appear unrealistically high.

FIGURE 10

The fit from model 1SHT matches the wavelength of the signal but produces a pronounced misfit in the area of maximum deformation (Fig. 10). To investigate this mismatch further we first ran a slightly modified model (1ScHT), which simulates the oblate source as before yet also includes a 300m thick compliant layer with a Young's modulus of 0.1 GPa located at the free surface to represent soft caldera fill material (Fig. 11). As shown in the previous section the presence of very soft layer at the surface could amplify considerably the resulting deformation. However, as model results depicted in Figure 10a demonstrate, we find that this amplification effect is minor and does not account for the observed near-range uplift data. In fact the quality of fit to the observables is only marginally improved (with χ^2 = 0.11) compared to the previous model (Fig. 10b)

FIGURE 11

We then investigated the effect of a second shallower source located above the main inflating reservoir (Fig. 11). Earlier works demonstrated that reservoir multiplicity can play an important role for local amplification of surface deformation in caldera settings with juxtaposition or superposition of individual reservoirs (Gottsmann et al, 2006 a,b; Geyer and Gottsmann, 2008). To test whether one obtains a better fit to both the near-field and far-field observations we ran several models modifying the size and depth of the second reservoir. We settled with a solution for a second source of length a = 1 km (width 2a = 2 km) and b = 50 m (height 2b = 100 m), with its upper surface

located at a depth of 1000 m and an uniformly distributed overpressure of 8MPa along the reservoir walls (Fig. 11). This model (2SHT) provides the best-fit with $\chi^2 = 0.7$ to the observations (Fig. 10b).

4.4. Discussion of Rabaul case study

Our best-fit model includes the superposition of two pressurised central sources with a cumulative pressure increment of 38 MPa. One may envisage a scenario of two hydrothermal sources or a hydrothermal source above a magmatic source.

An alternative model to explain the Rabaul uplift was presented in Saunders (2001, 2005) who proposed pressurisation along ring faults rather than pressurisation of a central reservoir due to the requirement of unreasonably high overpressures for the latter. We note here that it is on the grounds of oversimplifications in homogenous half-space models that leads one to reject a central reservoir as a causative source. Our first order evaluation provides a viable alternative explanation to the observed ground uplift.

We do not wish enter a discussion as to which scenario more likely caused the uplift over the investigated period (stress coupling in central reservoirs or intrusion into circumferential faults) other than to show that pressurisation of central reservoirs in a mechanically heterogeneous crust can equally well explain the reported ground deformation at Rabaul. We also note that the available ground deformation data from the Rabaul uplift does not indicate an influence of peripheral faults (ring faults) on the deformation pattern caused by a central source as the gradient between Δh and distance from source evolves smoothly without any perturbation. Deformation patterns caused by pressurised central reservoirs are found to be heavily distorted in the presence of ring faults (see for example Fig. 8 in Folch and Gottsmann, 2006; De Natale and Pingue, 1993).

Anelastic effects in mid-crustal reservoirs may play a role during caldera deformation, e.g., at Long Valley caldera (Newman 2006, 2009) or Campi Flegrei (Bianchi et al. 1987). Time-dependent mechanical behaviour predominantly results in a net decrease of required overpressure to fit observed deformation data. We show here that mechanical heterogeneity is a first-order variable influencing volcano deformation and it is expected that the combination of effects of both time-dependence and mechanical heterogeneity will have significant bearing on deduced overpressures. Particularly for the case shallow reservoirs as investigated here, however, time-dependent rheology may be of lesser importance than is perhaps anticipated as efficient cooling from hydrothermal/meteoric fluid circulation can significantly increase heat loss at depth (Nakada et al., 2005). Undoubtedly, this problem deserves further attention.

5. Summary and conclusions

The forward numerical models presented here enable the axi-symmetric simulation of the effect of host rock mechanical properties on ground deformation produced by pressurizing a subsurface source. Of course our models are equally applicable for the case of ground deflation and hence reservoir depressurization. Our models are particularly suitable to study ground deformation at calderas, where rock successions filling the collapse depression are likely to have different mechanical properties than surrounding host rock. In this sense, for the sake of the modelling, it is irrelevant whether the source is *a priori* seen as being of magmatic or hydrothermal nature. Clearly, ground deformation data alone is not indicative of the nature of the source(s) and thus other geodetic techniques such as gravity measurements need to

endorse ground deformation measurements to help inferring its (their) nature (Gottsmann and Battaglia, 2008; Battaglia et al., 2008).

The models presented here serve to demonstrate that the mechanical properties of the surrounding host rock and reservoir geometries measurably affect the resulting pattern of surface displacements and stress distributions around pressurized sources.

The main point to highlight is the strong influence of soft and stiff layers and their mutual distribution on the amplitude of surface deformation (both vertical and horizontal displacements). The effect becomes more pronounced with increased contrasts in the mechanical stiffness of encasing rocks.

Our study clearly identifies the need to better quantify mechanical properties of subsurface lithologies in volcanic areas. The applicability of numerical models to shed light on subsurface dynamics during volcano deformation appears currently most confined by our limited knowledge of realistic mechanical properties, the distribution and the possible time-dependent rheology of crustal rocks.

Acknowledgements

The research was support by Spanish MEC (grant 2007-0400), the Royal Society and NERC. We thank John C. Mutter, A. Folch and two anonymous reviewers for their suggestions that helped improve this manuscript.

References

Anderson, E.M., 1936. The dynamics of formation of cone sheets, ring dykes and cauldron subsidences. Proceedings of the Royal Society of Edinburgh, 56: 128-163

Battaglia, M., Gottsmann, J., Carbone, D. and Fernández, J., 2008. 4D Volcano gravimetry Geophysics Geophysics, 73(6): WA3-WA18.

Bianchi, R., Coradini, A., Federico, C., Giberti, G., Lancian, P., Pozzi, J.P., Sartoris, G. and Scandone, R., 1987. Modeling of surface deformation in volcanic areas: The 1970-1972 and 1982-1984 crises of Campi Flegrei, Italy. Journal of Geophysical Research, 92: 14139-14150.

Bonaccorso, A., Cianetti, S., Giunchi, C., Trasatti, E., Bonafede, M. and Boschi, E., 2005. Analytical and 3-D numerical modeling of mt. Etna (Italy) volcano inflation. Geophysical Journal International, 163: 852-862.

Bonafede, M., and Danesi, S., 1997. Near-field modifications of stress induced by dyke injection at shallow depth. Geophysical Journal International, 130: 435-448

Brocher, T., 2005. Empirical relations between elastic wavespeeds and density in the Earth's crust. Bulletin of the Seismological Society of America, 95(6): 2081-2092.

Codina, R. and Folch, A., 2004. A stabilized finite element predictor-corrector scheme for the incompressible Navier-Stoke equations using a nodal based implementation. International Journal of Numerical Methods in Fluids, 44: 483-503.

De Natale, G. and Pingue, F., 1992. Seismological and geodetic data at Campi Flegrei (Southern Italy) area: constraints on volcanological models. In: p. Gasparini, S. R.

and K. Aki (Editors), Volcanic Seismology. Procedures in Volcanology. IAVCEI, pp. 483-502.

De Natale, G. and Pingue, F., 1993. Ground deformations in collapsed caldera structures. Journal of Volcanology and Geothermal Research, 57: 19-38.

De Natale, G. and Pingue, F., 1996. Ground deformation modeling of volcanic areas. In: R. Scarpa and R.I. Tilling (Editors), Monitoring and Mitigation of Volcanic Hazards. Springer-Verlag, Berlin, pp. 365-388.

De Natale, G., Petrazzuoli, S.M. and Pingue, F., 1997. The effect of collapse structure on ground deformations in calderas. Geophysical Research Letters, 24: 1555-1558.

Dieterich, J.H. and Decker, R.W., 1975. Finite element modeling of surface deformation associated with volcanism. Journal of Geophysical Research, 80: 4094-4102.

Dzurisin, D. and Johnston, D.A., 2003. A comprehensive approach to monitoring volcano deformation as a window on the eruption cycle. Reviews of Geophysics, 41: doi: 10.1029/2001RG000107.

Fialko, Y., Khazan, Y. and Simons, M., 2001. Deformation due to a pressurized horizontal circular crack in an elastic half-space, with applications to volcano geodesy. Geophysical Journal International, 146: 181-191.

Finlayson, D.M., Gudmundsson, O., Itakarai, I., Nishimura, Y. and Shimamu, H., 2003. Rabaul volcano, Papua New Guinea: seismic tomographic imaging of an active caldera. Journal of Volcanology and Geothermal Research, 124: 153-171.

Folch, A. and Gottsmann, J., 2006. Volcanic unrest: Faults and uplift at active calderas. In: C. Troise, G. De Natale and C.R.J. Kilburn (Editors), Mechanisms of Activity and Unrest at Large Calderas. Geological Society of London, London, pp. 109-120.

Geyer, A. and Gottsmann, J., 2008. Ground deformation at collapse calderas: Influence of host rock lithology and reservoir multiplicity. IOP Conf. Series: Earth and Environmental Science, 3: 012017.doi:10.1088/1755-1307/3/1/012017

Gottsmann, J., A. Folch, and H. Rymer, 2006. Caldera unrest at Campi Flegrei: a contribution to the magmatic vs. hydrothermal debate from inverse and finite element modeling. Journal of Geophysical Research, Vol. 111, No. B7, B07203, 10.1029/2005JB003745.

Gottsmann J, Camacho A, Fernandez J, Tiampo KF (2006) Spatio-temporal variations in vertical gravity gradients at the Campi Flegrei caldera (Italy): A case for source multiplicity during unrest? Geophysical Journal International 167:1089-1096

Gottsmann, J. and Battaglia, M., 2008. Deciphering causes of unrest at collapse calderas: Recent advances and future challenges of joint gravimetric and ground deformation studies. . In: J. Gottsmann and J. Martí (Editors), Caldera volcanism: Analysis, modelling and response. . Developments in Volcanology. Elsevier, pp. 417-446.

Gudmundsson, A., 2006. How local stresses control magma-chamber ruptures, dyke injections, and eruptions in composite volcanoes Earth-Science Reviews, 79(1-2), 1-31.doi: 10.1016/j.earscirev.2006.06.006

Gudmundsson, A., 2007. Conceptual and numerical models of ring-fault formation. Journal of Volcanology and Geothermal Research, 164: 142-160.

Gudmundsson, A. and Brenner, S.L., 2004. How mechanical layering affects local stresses, unrests, and eruptions of volcanoes. Geophysical Research Letters, 31, L16606.doi:10.1029/2004GL020083

Heming, R.F. and Carmichael, I.S.E., 1973. High-temperature pumice flows from the Rabaul Caldera Papua. Contributions to Mineralogy and Petrology, 38: 1-20.

Heming, R.F., 1974. Geology and petrology of Rabaul caldera, Papua New Guinea. Geological Society of America Bulletin, 85: 1253-1264.

Heming, R.F., 1977. Mineralogy and proposed P-Tpaths of basalticlavas from Rabaul Caldera, Papua New Guinea. . Contributions to Mineralogy and Petrology, 61: 15-33.

Masterlark, T., 2007. Magma intrusion and deformation predictions: Sensitivities to the Mogi assumptions. Journal of Geophysical Research, 112(B06419): doi: 10.1029/2006JB004860.

McKee, C., Lowenstein, P.L., De Saint Ours, P., Talai, B., Itakarai, I. and Mori, J.J., 1984. Seismic and ground deformation crisis at Rabaul Caldera: prelude to an eruption? . Bulletin of Volcanology, 47: 397-411.

McKee, C.O., Johnson, R.W., Lowenstein, P.L., Riley, S.J., Blong, R.J., De Saint Ours, P. and Talai, B., 1985. Rabaul Caldera, Papua New Guinea: Volcanic hazards, surveillance, and eruption contingency planning. Journal of Volcanology and Geothermal Research, 23(3-4): 195-237.

Melan, E., 1932. Point force at internal point in a semi-infinite plate. Z. Angew. Math. Mech., 12: 343-346 (in German)

Mindlin, R.D., 1936. Force at a point in the interior of a semi-infinite solid. Physics, 7: 195-202

Mogi, K., 1958. Relations of the eruptions of various volcanoes and the deformations of the ground surface around them. Bulletin of the Earthquake Research Institute University of Tokio, 36: 99-134.

Nairn, I.A., McKee, C.O., Talai, B. and Wood, C.P., 1995. Geology and eruptive history of the Rabaul caldera area , Papua New Guinea. Journal of Volcanology and Geothermal Research, 69: 255-284.

Nakada, S., Uto, K., Sakuma, S., Eichelberger, J.C., Shimizu, H., 2005. Scientific Results of Conduit Drilling in the Unzen Scientific Drilling Project (USDP). Scientific Drilling, 1(2005):18-22.doi:10.2204/iodp.sd.1.03.2005.

Newman, A.V., Dixon, T.H., Ofoegbu, G.I. and Dixon, J.E., 2001. Geodetic and seismic constraints on recent activity at Long Valley Caldera, California: Evidence for viscoelastic rheology. Journal of Volcanology and Geothermal Research, 105: 183-206.

Newman, A.V., Dixon, T.H. and Gourmelen, N., 2006. A four-dimensional viscoelastic deformation model for Long Valley Caldera, between 1995 and 2000. Journal of Volcanology and Geothermal Research, 150: 244-269.

Okada, Y., 1985. Surface deformation due to shear and tensile faults in a half-space. Bulletin of the Seismological Society of America, 75: 1135-1154.

Okada, Y., 1992. Internal deformation due to shear and tensile faults in a half-space. Bulletin of the Seismological Society of America, 82(2): 1018-1040.

Orsi, G., Petrazzuoli, S.M. and Wohletz, K., 1999. Mechanical and thermofluid behavior during unrest at the Campi Flegrei caldera (Italy). Journal of Volcanology and Geothermal Research, 91: 453-470.

Poland, M.R., Bürgmann, R., Dzurisin, D., Lisowski, M., Masterlark, T., Owen, S. and Fink, J., 2006a. Constraints on the mechanism of long-term, steady subsidence at Medicine Lake volcano, northern California, from GPS and precise leveling. Journal of Volcanology and Geothermal Research, 150: 55-78.

Poland, M.R., Hamburger, M. and Newman, A., 2006b. The changing shapes of active volcanoes: History, evolution, and future challenges for volcano geodesy. Journal of Volcanology and Geothermal Research, , The Changing Shapes of Active Volcanoes - Recent Results and Advances in Volcano Geodesy, 150: 1-3.

Saunders, S.J., 2001. The shallow plumbing system of Rabaul caldera: a partially intruded ring fault? Bulletin of Volcanology, 63: 406-420.DOI 10.1007/s004450100159

Saunders, S.J., 2005. The possible contribution of circumferential fault intrusion to caldera resurgence. Bulletin of Volcanology, 67: 57-71.DOI 10.1007/s00445-004-0360-z

Trasatti, E., Giunchi, C. and Bonafede, M., 2003. Effects of topography and rheological layering on ground deformation in volcanic regions. Journal of Volcanology and Geothermal Research, 122: 89-110.

Troise, C., Pingue, F. and De Natale, G., 2003. Coulomb stress changes at calderas: Modeling the seismicity of Campi Flegrei (southern Italy). Journal of Geophysical Research, 108(B6): 4-1/4-11.

Troise, C., De Natale, G., Pingue, F., Tammaro, U., De Martino, P., F., O. and Boschi, E., 2008. A new uplift episode at Campi Flegrei caldera (Southern Italy): implications for unrest interpretation and eruption hazard evaluation. In: J. Gottsmann and J. Marti (Editors), Volcanic calderas: Analysis, Modelling and Response. Developments in Volcanology. Elsevier, Amsterdam, pp. 336.

Vasco, D.W., Johnson, L.R. and Goldstein, N.E., 1988. Using surface displacement and strain observations to determine deformation at depth, with application to Long Valley caldera, California. Journal of Geophysical Research, 93(B4): 323-3242.

Walsh, J.B. and Decker, R.W., 1971. Surface deformation associated with volcanism. Journal of Geophysical Research, 76: 3291.

Williams, C.A. and Wadge, G., 1998. The effects of topography on magma chamber deformation models: Application to Mt Etna and radar interferometry. Geophysical Research Letters, 25: 1549-1552.

Wood, C.P., Nairn, I.A., McKee, C. and Talai, B., 1995. Petrology of Rabaul Caldera, Papua New Guinea. Journal of Volcanology and Geothermal Research, 69: 289-306.

Yang, X.M., Davies, P.M. and Dieterich, J.H., 1988. Deformation from inflation of a dipping finite prolate spheroid in an elastic half-space as a model for volcanic stressing. Journal of Geophysical Research, 93: 4249-4257.

Figure captions

Fig. 1: (a) Representation of the computational domain (grey) with the reservoir located at a certain depth. The reservoir used in these numerical models is characterized by two semi-axes *a* and *b* Boundary conditions have been also illustrated. The reservoir has an overpressure ΔP imposed at the reservoir walls. The value of ΔP depends on the numerical model (Table 2). The Earth's surface is treated as a free surface (i.e. traction free) and the computational margins are fixed, i.e. zero displacement. (b) Sketch of the configuration of the performed models. In order to introduce heterogeneities in the model we define seven 500m thick layers between 1000m and 4500m depth. If the host rock is considered to be homogeneous all layers have the same mechanical properties. Contrarily, by assigning different mechanical properties to the individual layers the host rock becomes heterogeneous.

Fig. 2: Sketch of the performed models. The code system is in agreement with the one of Tables 1 and 2.

Fig. 3: Results for those numerical runs assuming different thicknesses for the soft and stiff layer (T_{SL} and T_{HL}, respectively). (a) and (b) vertical displacement u_{yy} at surface; (c) and (d) horizontal displacement u_{xx} at surface; (e) and (f) normalized vertical displacement u_{yy} at surface; (g) and (h) normalized horizontal displacement u_{xx} at surface. Thick dashed line/curves correspond to the homogeneous results.

Fig. 4: Results for those numerical runs assuming different thicknesses for the soft layer and the stiff layer (RLT). (a) and (b) vertical displacement u_{yy} at surface; (c) and (d)

horizontal displacement u_{xx} at surface; (e) and (f) normalized vertical displacement u_{yy} at surface; (g) and (h) normalized horizontal displacement u_{xx} at surface. Thick dashed line/curves correspond to the homogeneous results.

Fig. 5: Results for those numerical runs assuming different distance between the soft layer and the stiff layer (DL). (a) and (b) vertical displacement u_{yy} at surface; (c) and (d) horizontal displacement u_{xx} at surface; (e) and (f) normalized vertical displacement u_{yy} at surface; (g) and (h) normalized horizontal displacement u_{xx} at surface. Thick dashed line/curves correspond to the homogeneous results.

Fig. 6: Results for those numerical runs assuming different distribution pattern for the stiff layers (LDP). (a) and (b) vertical displacement u_{yy} at surface; (c) and (d) horizontal displacement u_{xx} at surface; (e) and (f) normalized vertical displacement u_{yy} at surface; (g) and (h) normalized horizontal displacement u_{xx} at surface. Thick dashed line/curves correspond to the homogeneous results.

Fig. 7: Ratio between the maximum horizontal and the maximum vertical displacement at surface, i.e. $u_{xx}\max / u_{yy}\max$. for the different models. Thick dashed lines correspond to the homogeneous results. See text for more details.

Fig. 8: (a) Location of Rabaul caldera on the island of New Britain, Papua New Guinea (left) and false-colour radar image of the Rabaul caldera. The image is centred at 4.2 degrees South and 152.2 degrees East. The area shown is approximately 21 × 25 kilometres (source of basemap: http://www.nasaimages.org). Locations of volcanic cones Taravur and Vulcan and Matupit Island are depicted as well as the approximate

rim of the caldera. (b) Velocity model by Finlayson et al. (2003). These authors remark the deepening of the relative low-velocity region (< 5.0 km/s) in the centre of the caldera, considered to be the location of a low-velocity magmatic reservoir at depths of 3-5 km. c) Uplift recorded via levelling versus distance from the inflation centre near Matupit Island during the period November 1971-March 1984. After McKee et at. (1985)

Fig. 9: Sketch of the configuration of the performed models. Boundary conditions are also included. Mechanical properties of the different materials considered are obtained from p-wave velocities (V_p) using Equations 1-3 and the data reported in Finlayson et al. (2003). See text for more details.

Fig. 10: a) Uplift recorded via levelling versus distance from the inflation centre near Matupit Island (after McKee et at. (1985)) and fits to observables from forward models assuming an isotropic elastic homogeneity and elastic heterogeneity. b) Fit residuals from model simulations (1SHO, 1SHT, 1ScHT and 2SHT; see also Fig. 11) as a function of benchmark distance from inflation centre.

Fig.11: Sketch of two alternative models for the Rabaul case study. I) Model 1ScHT equivalent to the one of Figure 9 but it includes a 300m thick compliant layer with a Young's modulus of 0.1 GPa located at the free surface to represent soft caldera fill material. II) Model 2SHT considering a second source of length a = 1 km (width $2a$ = 2 km) and b = 50 m (height $2b$ = 100 m), with its upper surface located at a depth of 1000 m and an uniformly distributed overpressure of 8MPa along the reservoir walls.

Table captions

Table 1: List of parameters and variables

Table 2: List of performed numerical runs. . For all the models, the magma chamber is located at 3 km depth and ΔP = 15 MPa, a=5 km and b=1.5 km. ; **DL** Distance between the soft and stiff layer; **Mat** Material; $\mathbf{T_{HL}}$ Thickness of the stiff layer; $\mathbf{T_{SL}}$ Thickness of soft layers. The notation is the same as in Fig.2; thus, 1,2,3 indicates that all three layer properties (listed in Fig. 2, bottom) are used.

FIGURE 1

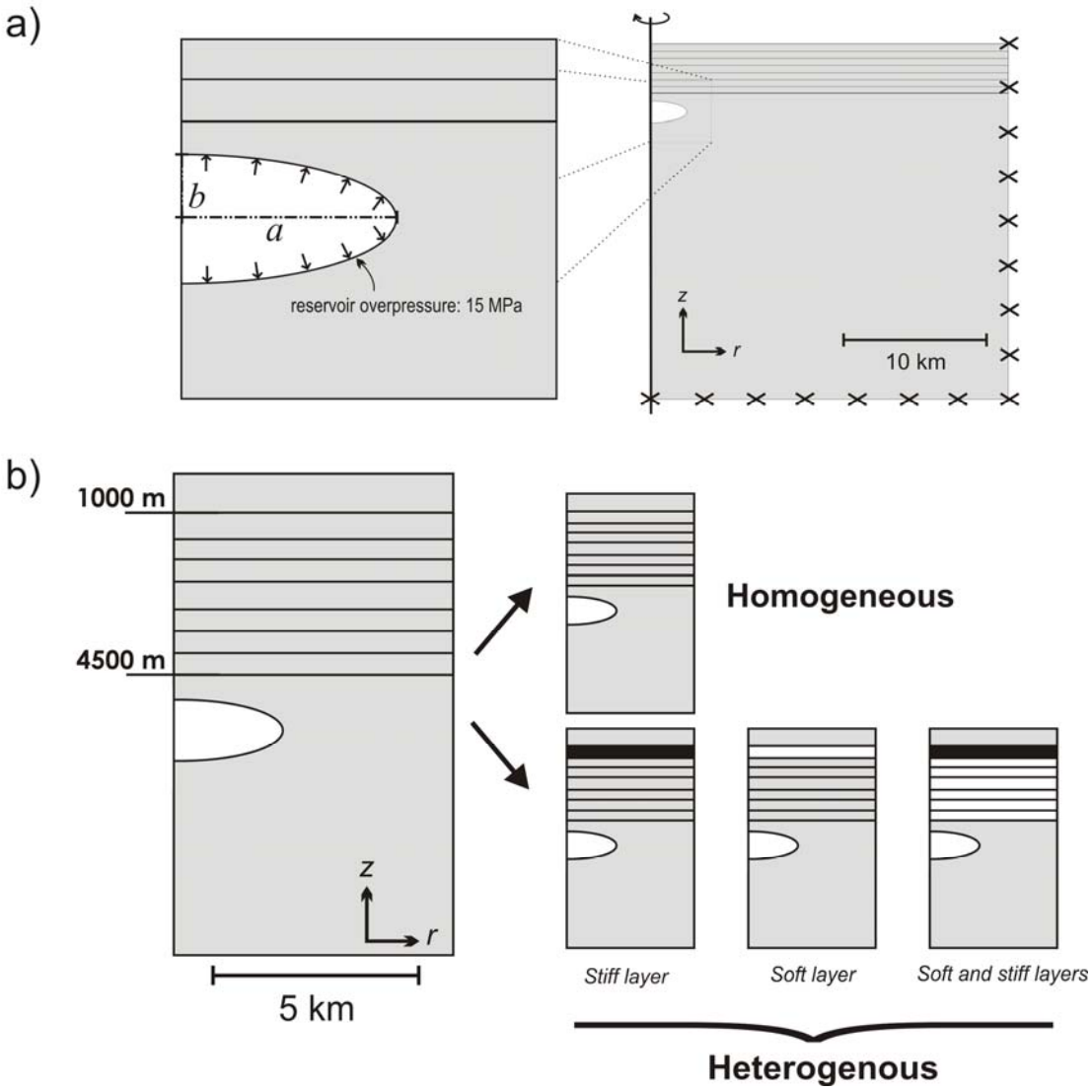

FIGURE 2

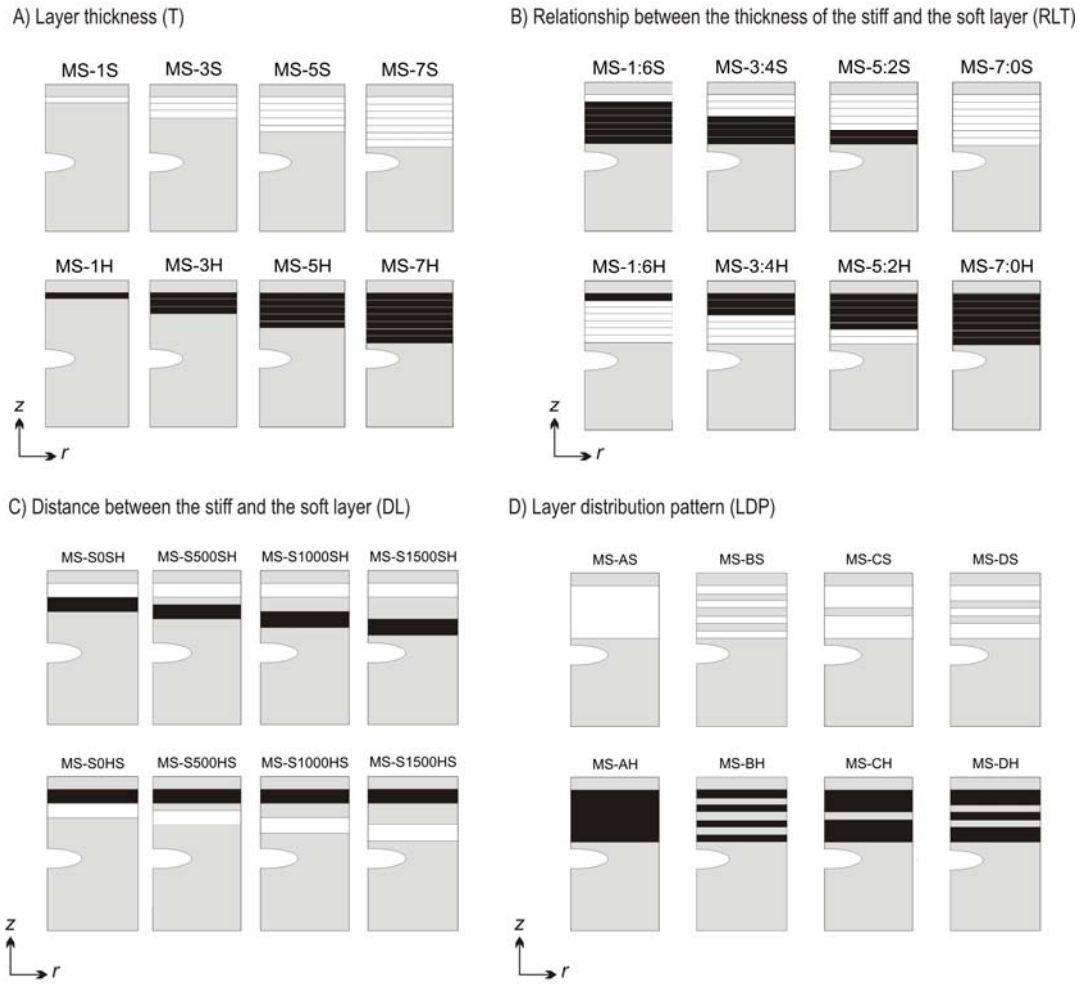

FIGURE 3

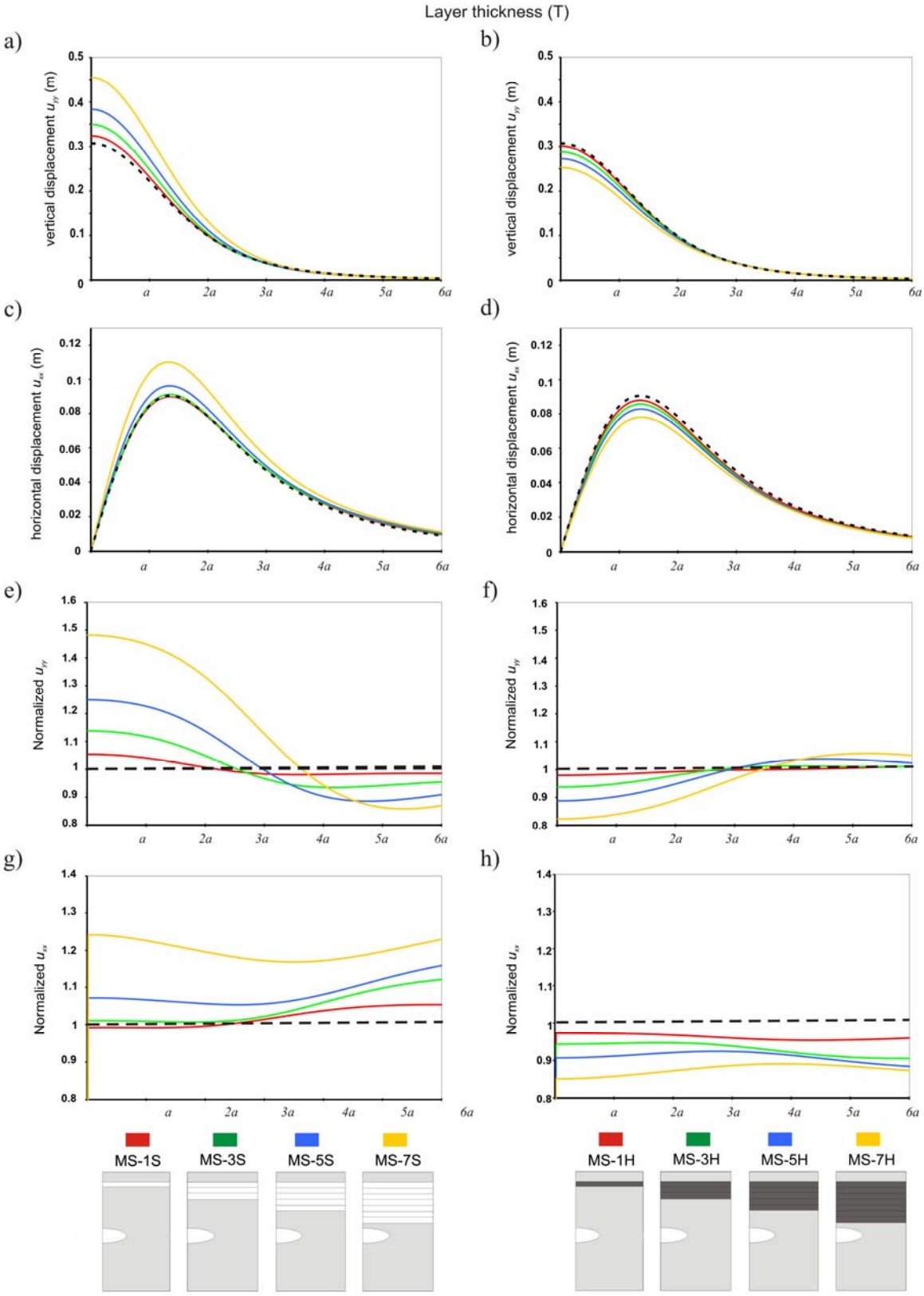

FIGURE 4

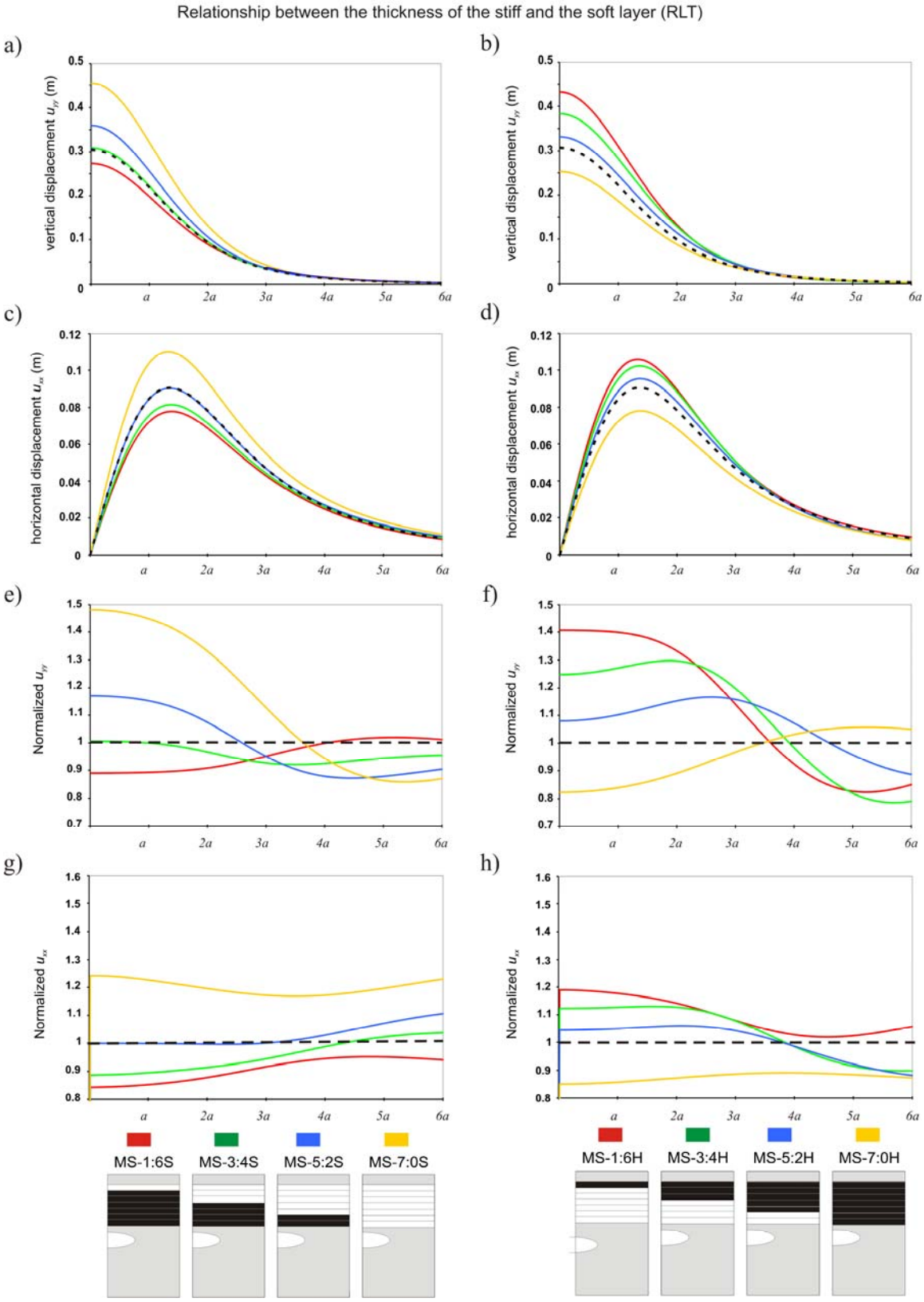

FIGURE 5

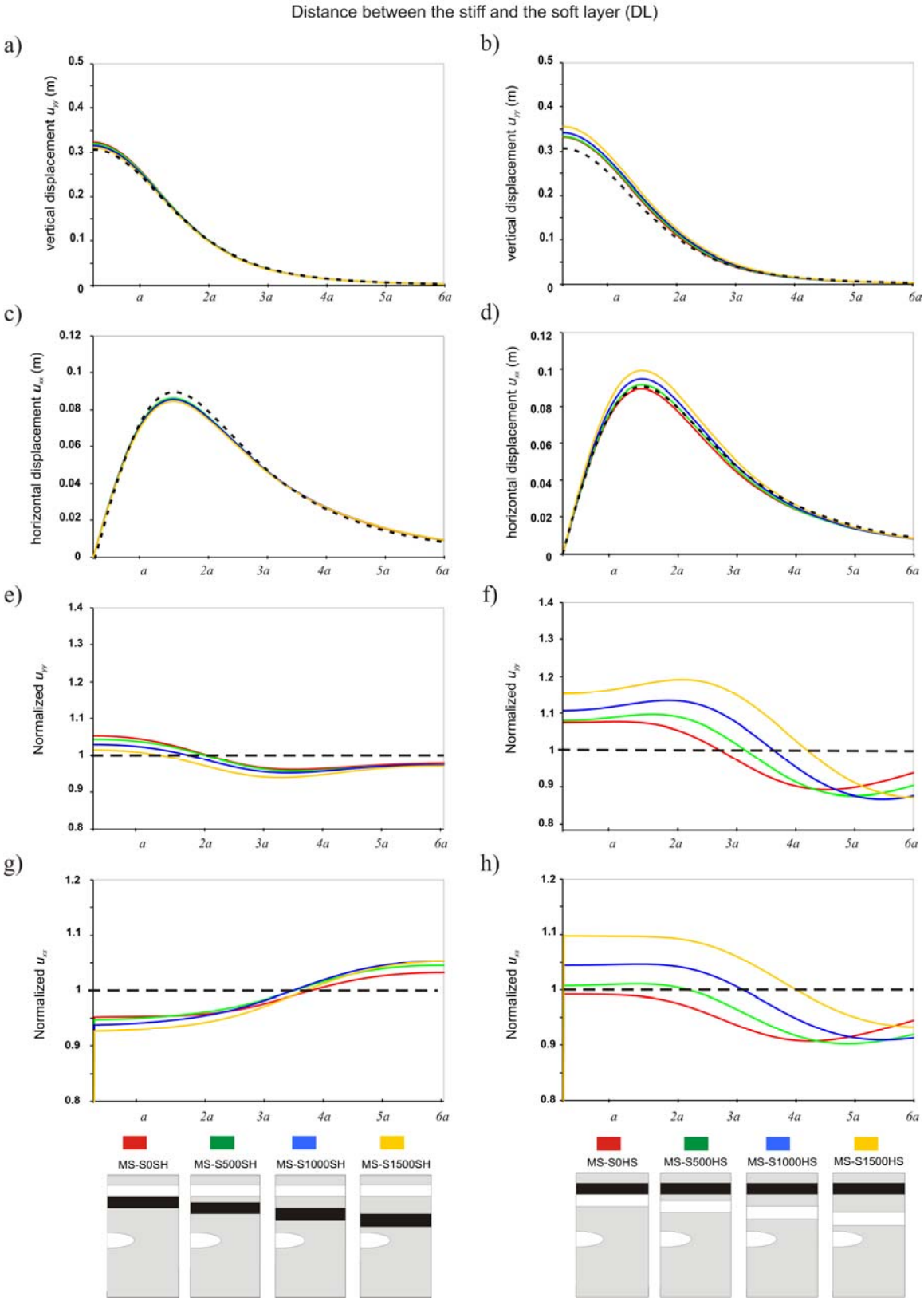

FIGURE 6

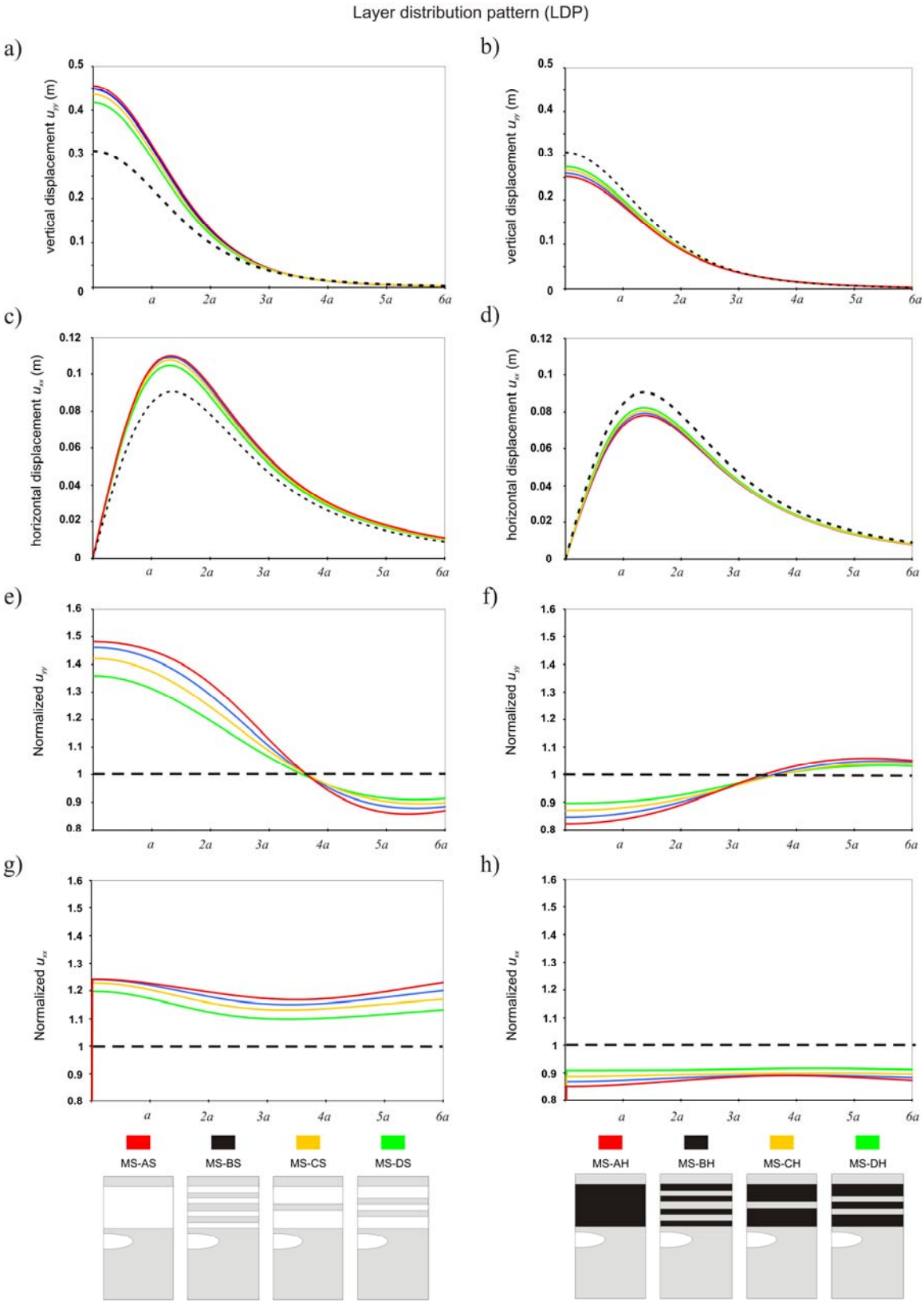

FIGURE 7

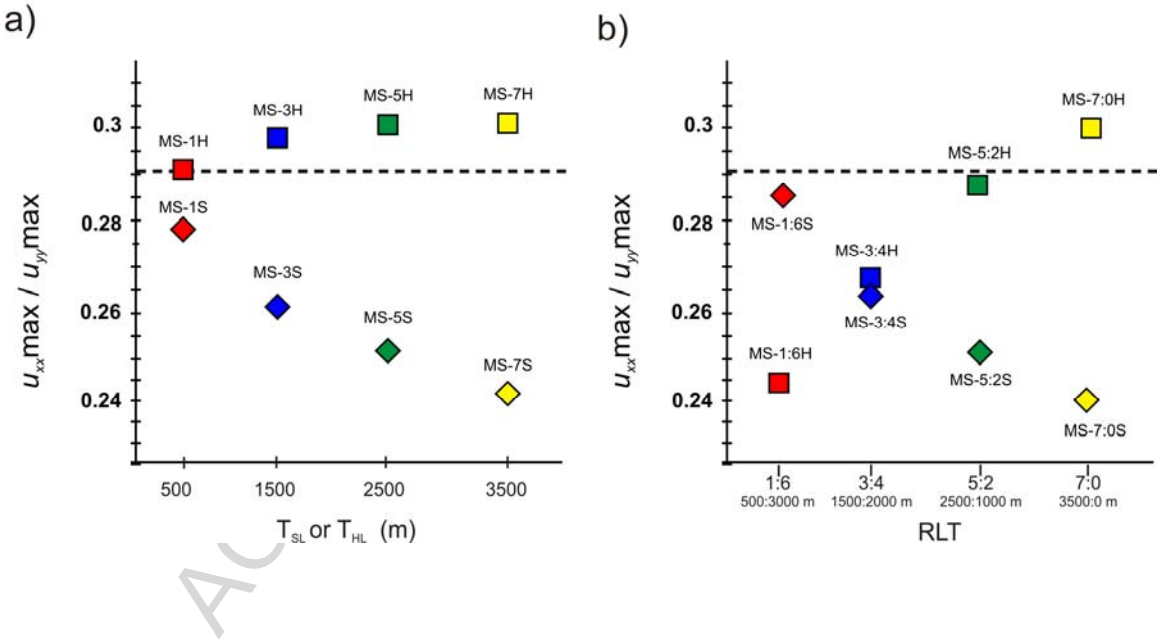

FIGURE 8

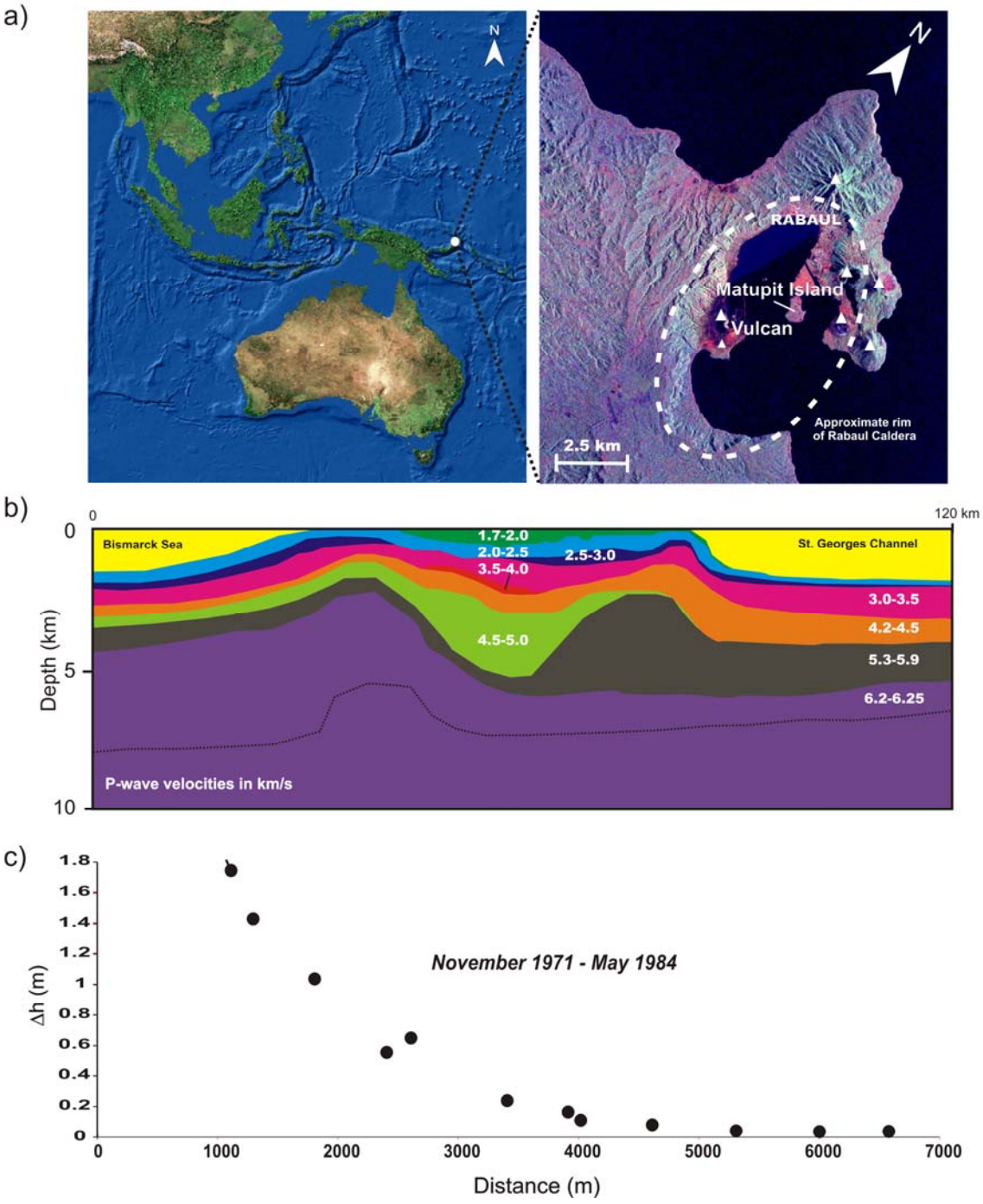

FIGURE 9

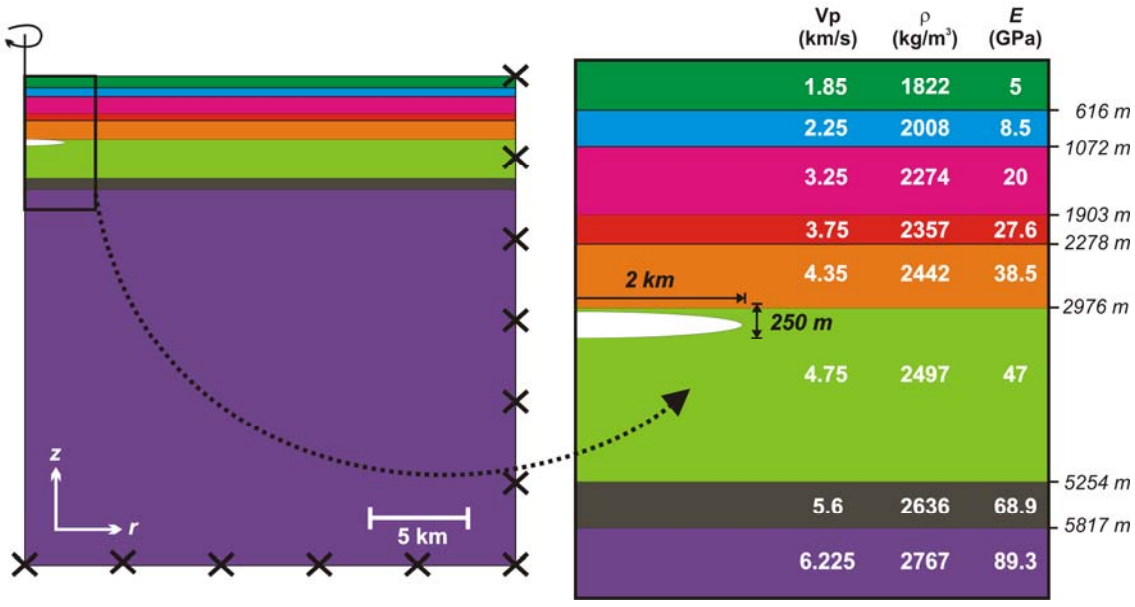

FIGURE 10

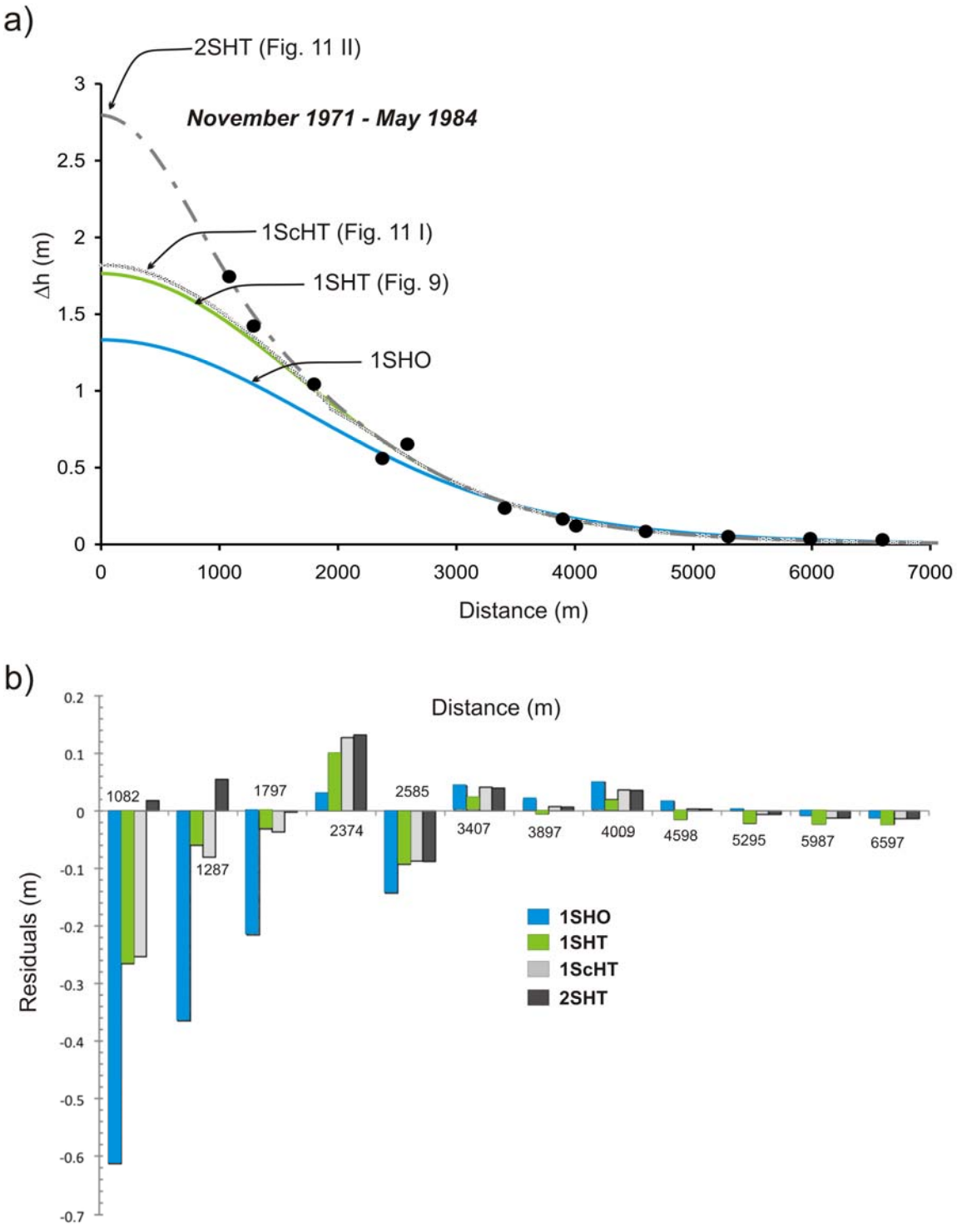

FIGURE 11

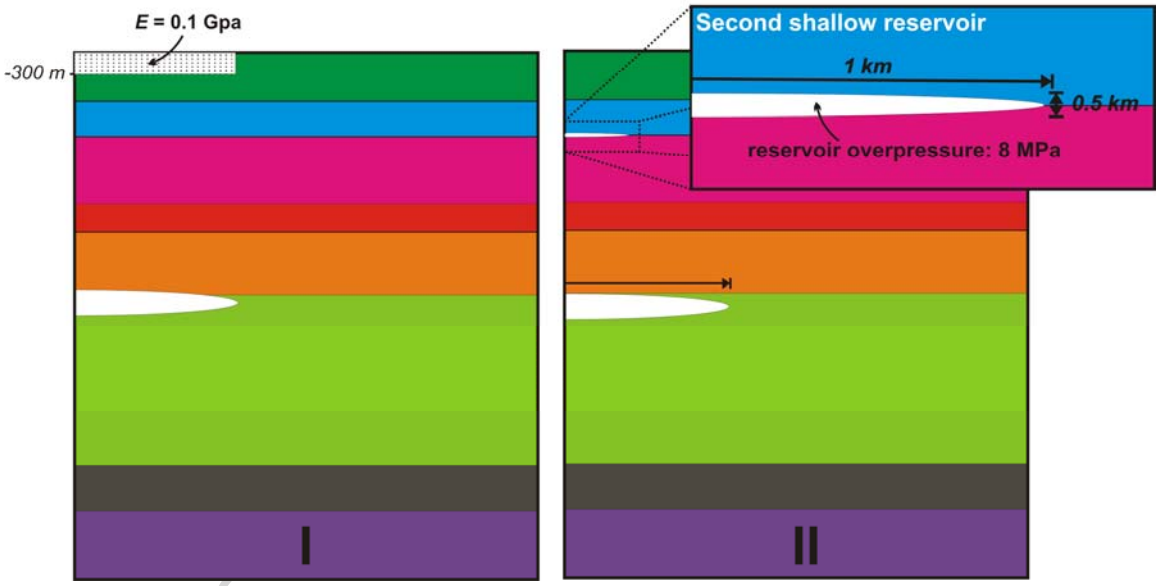

TABLE 1

Variable	Definition	Dimensions
a	Horizontal axis of the reservoir	m
b	Vertical axis of the reservoir	m
ΔP	Internal excess pressure (overpressure) of the reservoir	Pa
DL	Distance between soft and stiff layer	m
E	Young's Modulus	Pa
LDP	Layer distribution pattern	--
RLT	Ratio between the thicknesses of soft and stiff layers	--
T	Layer thickness	m
T_{SL}	Thickness of the soft layer	m
T_{HL}	Thickness of the stiff layer	m
u_{xx}	Theoretical horizontal displacement at surface	m
u_{yy}	Theoretical vertical displacement at surface	m
$u_{xx\mathrm{HOMO}}$	Theoretical horizontal displacement at surface for the homogeneous model	m
$u_{yy\mathrm{HOMO}}$	Theoretical vertical displacement at surface for the homogeneous model	m
$u_{xx\mathrm{max}}$	Maximum theoretical horizontal displacement at surface	m
$u_{yy\mathrm{max}}$	Maximum theoretical vertical displacement at surface	m
ν	Poisson's ratio	--

TABLE 2

Mod	Mat	T_{SL} (km)	T_{HL} (km)	DL (km)
MS-1S	1,2	0.5	----	----
MS-3S	1,2	1.5	----	----
MS-5S	1,2	2.5	----	----
MS-7S	1,2	3.5	----	----
MS-1H	1,2	----	0.5	----
MS-3H	1,3	----	1.5	----
MS-5H	1,3	----	2.5	----
MS-7H	1,3	----	3.5	----
MS-1:6S	1,2,3	0.5	3	0
MS-3:4S	1,2,3	1.5	2	0
MS-5:2S	1,2,3	2.5	1	0
MS-7:0S	1,2,3	3.5	----	----
MS-1:6H	1,2,3	3	0.5	0
MS-3:4H	1,2,3	2	1.5	0
MS-5:2H	1,2,3	1	2.5	0
MS-7:0H	1,2,3	----	3.5	----
MS-S0SH	1,2,3	0.5	0.5	0
MS-S500SH	1,2,3	0.5	0.5	0.5
MS-S1000SH	1,2,3	0.5	0.5	1
MS-S1500SH	1,2,3	0.5	0.5	1.5
MS-S0HS	1,2,3	0.5	0.5	0
MS-S500HS	1,2,3	0.5	0.5	0.5
MS-S1000HS	1,2,3	0.5	0.5	1
MS-S1500HS	1,2,3	0.5	0.5	1.5
MS-AS	1,2	3.5	----	----
MS-BS	1,2	4×0.5	----	----
MS-CS	1,2	2×1.5	----	----
MS-DS	1,2	$2 \times 1 + 1 \times 0.5$	----	----
MS-AH	1,3	----	3.5	----
MS-BH	1,3	----	4×0.5	----
MS-CH	1,3	----	2×1.5	----
MS-DH	1,3	----	2×1	----